Leckie, R.M., Sigurdsson, H., Acton, G.D., and Draper, G. (Eds.), 2000
Proceedings of the Ocean Drilling Program, Scientific Results, Vol. 165

10. INTERPRETATION OF BURIAL HISTORY AND REBOUND FROM LOADING EXPERIMENTS AND OCCURRENCE OF MICROSTYLOLITES IN MIXED SEDIMENTS OF CARIBBEAN SITES 999 AND 1001[1]

Ida L. Fabricius[2]

ABSTRACT

Compaction curves for 11 samples from the mixed sediments and calcareous chalk with clay from the Caribbean Sites 999 and 1001 are discussed with reference to compaction curves for calcareous ooze and chalk of the Ontong Java Plateau (Leg 130). The burial history is discussed from preconsolidation data and present burial conditions and suggests a removal of ~400 m of sediment at the hiatus 166 meters below seafloor (mbsf) at Site 1001. This interpretation predicts a previous burial to >500 mbsf for depth intervals containing microstylolites, which corresponds to observations at Sites 999 and 807 (Ontong Java Plateau). Thus, data from three sites from two widely separate regions indicate that microstylolites in carbonates form at minimum burial depths deeper than 500 m. No direct link between formation of microstylolites and cementation was found, suggesting that dissolution and precipitation are not necessarily related. Porosity rebound during core retrieval could not be detected for soft sediments, whereas a porosity rebound of ~2% was deduced for deeper, cemented intervals.

Comparing the compaction curves, two distinct rates of porosity loss are noted: (1) samples dominated by clay (>45% insoluble residue) compact at a higher rate than samples dominated by fine-grained carbonate and (2) fine-grained carbonate-supported samples (with <45% insoluble residue) compact at the same rate irrespective of the content of nonsupporting microfossils or pore-filling clay.

INTRODUCTION

The burial diagenesis of calcareous sediments has been widely studied (e.g., Schlanger and Douglas, 1974; Scholle, 1977; Maliva and Dickson, 1992; Borre and Fabricius, 1998) and linked to geotechnical properties (e.g., Hamilton, 1976; Lind, 1993a; Audet, 1995) or acoustic velocities and physical properties (e.g., Mayer, 1979; Hamilton et al., 1982; Kim et al., 1985; Urmos et al., 1993). The aim of the present paper is to compare compaction properties for the mixed sediments of the Caribbean to compaction curves obtained in a pure carbonate lithology, primarily from the Ontong Java Plateau, to interpret the role of textural differences and burial history. The role of rebound of core material after removal from in situ conditions is also discussed. Caribbean Leg 165 Sites 999 and 1001 were chosen because they both penetrated long sections of pelagic clayey mixed sediments. Leg 130 Site 807 from the calcareous sediments of the Ontong Java Plateau was selected as a reference.

The differences in diagenetic history of the three sites is immediately apparent by comparing the velocity-depth trends (Fig. 1). The sonic velocities indicate soft sediments down to a depth of ~570 meters below seafloor (mbsf) at Site 999, down to ~170 mbsf at Site 1001, and down to ~1100 mbsf at Site 807. Below these depths, the sonic velocity indicates indurated lithologies. Differences in burial history may be determined from preconsolidation measured by loading experiments and from the occurrence of stylolites.

As shown by Jacobsen (1972), preconsolidation is difficult to assess from consolidation tests. This difficulty is illustrated by data on the overconsolidation ratio (OCR) of Masters and Maghnani (1993) and Moran (1997). OCR is the ratio between the preconsolidation stress and the present effective overburden stress. OCR data for calcareous ooze of the Ontong Java Plateau range between 0.7 and 3.6 (Masters and Maghnani, 1993). OCRs of 0.3–0.5 for calcareous ooze of the Ceara Rise (Moran, 1997) suggest that the ooze is underconsolidated to a surprising degree.

An independent estimate of previous burial may be obtained from the occurrence of wispy lamination or flaser structures, which may be interpreted as solution seams (Garrison and Kennedy, 1977). They typically form as microstylolitic swarms in limestones containing >8%–10% clay, whereas in purer limestones, stylolites form (Bathurst, 1987). At the Ontong Java Plateau, wispy laminations were observed below 490 mbsf at Site 807 and below 630 mbsf at Site 806 (Kroenke, Berger, Janecek, et al., 1991; Lind, 1993b), and macroscopic stylolites below a burial of 830 mbsf at Site 807 (Lind, 1993b).

The physical properties measured in the laboratory will differ from in situ values if the core material expands as a result of the stress release during core retrieval. This rebound may be assessed from consolidation tests. Hamilton (1976) described a procedure to estimate rebound from the unloading part of compaction curves. For calcareous sediments he found a rebound (increase) in porosity ranging from zero near the seafloor to 5% at a depth of 500 mbsf, whereas for pelagic clay, he found a larger rebound (increase) in porosity ranging from zero near the seafloor to 7% at a depth of 300 mbsf. In general accordance with these results, Moran (1997) found a porosity rebound of 6% at a depth of 300 mbsf for the calcareous sediments of the Ceara Rise, and Masters and Maghnani (1993) found a rebound in porosity ranging from 1% to 4% in calcareous ooze of the Ontong Java Plateau (Leg 130). By contrast, using a compaction cell designed for high stresses, Lind (1993a) found a rebound of <0.1% for the calcareous ooze and chalk of the Ontong Java Plateau down to depths of 945 mbsf. This difference may be attributed to a difference in elasticity of the applied apparatus. If the compaction cell by itself has a significant bedding and deforms elastically, it becomes difficult to distinguish bedding of the apparatus from elastic deformation of the sample. Hamilton (1976), Masters and Maghnani (1993), and Moran (1997) used oedometers, which may imply significant bedding of the compaction cell (Jacobsen, 1972). This problem may have been overcome in the high-stress instrument used by Lind (1993a) and in the present study.

[1]Leckie, R.M., Sigurdsson, H., Acton, G.D., and Draper, G. (Eds.), 2000. *Proc. ODP, Sci. Results,* 165: College Station, TX (Ocean Drilling Program).

[2]Institut for Geologi og Geoteknik, Danmarks Tekniske Universitet, Bygning 204, DK-2800 Lyngby, Denmark. iggill@pop.dtu.dk

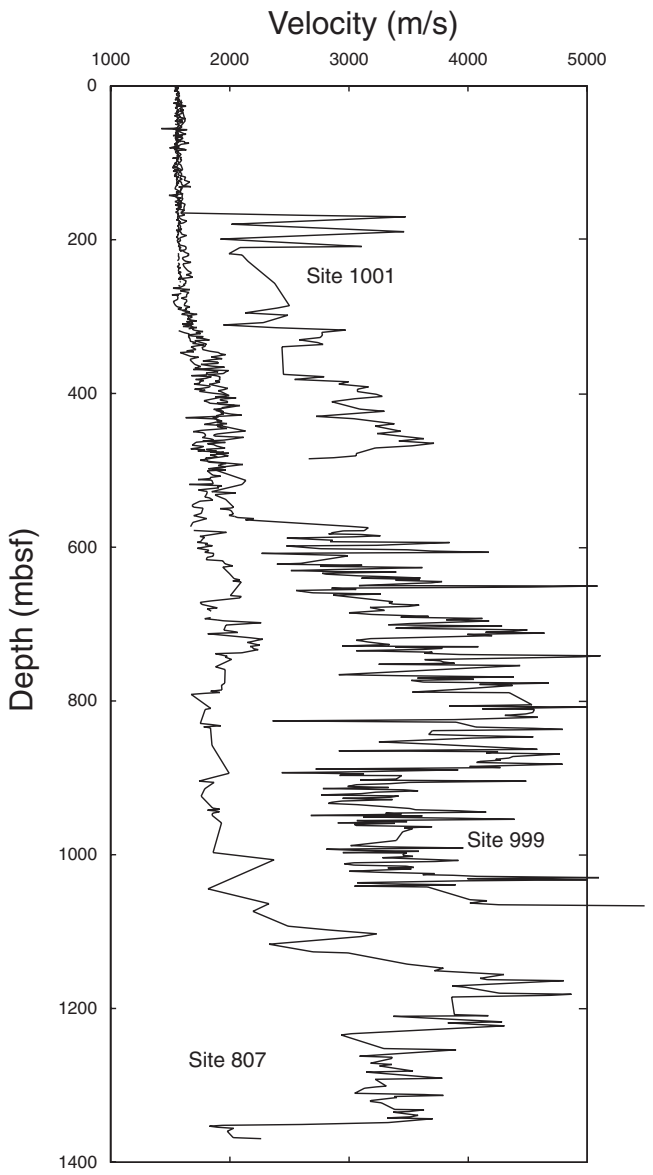

Figure 1. Sonic velocity of discrete freshly recovered (water saturated) samples vs. burial for Sites 999, 1001, and 807 (data from Kroenke, Berger, Janecek, et al., 1991, and Sigurdsson, Leckie, Acton, et al., 1997).

METHODS

Samples for the compaction experiments were collected as whole-round, 6-cm-long core sections sampled shortly after core recovery. Sedimentological descriptions of the sampled core sections are given in Table 1. The samples were kept in capped pieces of liner to avoid damage and change of shape. The liners were sealed in wax to avoid drying. The samples were stored in a refrigerator on board ship and again in a refrigerator after being hand carried to the laboratory. Samples for the experiments were cut using a steel pipe in the soft ooze, whereas samples from the more indurated sediments were drilled out of the core sections into vertical cylinders, 2.5 cm in diameter and 5 cm in length. The samples were kept in a closed humid box in a refrigerator, and the experiments were run within a week after cutting or drilling the samples.

All tests were uniaxially confined and conducted in a stainless-steel compaction cell (Lind, 1993a) with constant rate of strain (1–3.5 10^{-6} s^{-1}; Table 2) and one-sided parallel draining. The cell was equipped with a fluid pressure monitoring system, and the pore pressure was measured at the undrained end to ensure that the strain rate was low enough to prevent pore pressure build up. Two external, linear voltage deformation transducers were used. All experiments were done at room temperature. The loading was conducted to a maximal uniaxial effective stress of 10–42 MPa and a maximal uniaxial strain of 4%–42% (Table 2) and subsequently unloaded. Because sample disturbance was considered to be small, no strategy (e.g., repeated loading and unloading) was followed to overcome bedding. The unloading curve describing the final part of each test was only fully recorded for two samples because of software failure.

After the tests, the samples were carefully removed from the compaction cell, and the final unloaded strain was measured by a caliper. From each strained sample, a vertically oriented thin section was prepared from one half of the cylinder and described (Table 1; Pls. 1, 2). The other half was used for physical and chemical characterization (Table 3). The specific surface was measured by nitrogen adsorption according to the Brunauer, Emmett, and Teller (BET) method (see Brunauer et al., 1938) using a Micromeritics Gemini 2375. Multipoint as well as single-point data were recorded. The material was disintegrated by a treatment with sodium pyrophosphate, and the grain-size distribution was determined using a Micromeritics SediGraph 5100. The insoluble residue was measured after treatment with diluted hydrochloric acid. BET data were also recorded for the samples from Site 807 used for compaction experiments by Lind (1993a) (Table 4).

RESULTS AND DISCUSSION

The compaction curves follow the classical pattern for constant rate of strain tests: following a stress interval with elastic deformation, each sample reaches in situ stress or maximal prior stress, yields, and enters the normal-consolidated interval, where it undergoes plastic pore collapse (Fig. 2A, 2B). If the test is continued to high strains, work hardening sets in (Fig. 2A). To compare the textural changes in the studied samples, the compaction curves are recalculated to strain vs. porosity, and different consolidation curves are obtained (Figs. 3, 4).

In the following sections the compaction curves are discussed with regard to three aspects: (1) rebound of core material after removal from its natural position, (2) natural stress history of the material cored at Sites 999 and 1001, and (3) textural interpretation of the form of the compaction curves.

Rebound

In the present study, unloading curves were recorded for a few samples (Figs. 3, 4), but a possible rebound effect is discussed by comparing the final porosity measured from the dimensions of the sample when removed from the test chamber to the porosity calculated from the maximal strain observed during testing. The difference in porosity (*Final* φ – φ *at* ε *max*) is recalculated to φ *rebound* by dividing by the maximal testing stress (σ *max*) and multiplying by the *in situ stress* (Table 2), following the method of Hamilton (1976).

The estimated rebound in porosity has similar depth trends for Sites 999 and 1001 and ranges from zero near the seafloor to 1.9% at a depth of 459 mbsf. These values are larger than those reported by Lind (1993a) following the Hamilton method for samples from the Ontong Java Plateau, but smaller than those reported by Hamilton (1976), Moran (1997), and Masters and Maghnani (1993). These data suggest that no significant rebound effects are present in the most porous upper section of Sites 999 and 1001, whereas a rebound in porosity of ~2% may be expected in the cemented, deeper sections below 572 mbsf at Site 999 and below 352 mbsf at Site 1001.

Table 1. Lithological description of samples, Sites 999 and 1001.

Core, section, interval (cm)	Depth (mbsf)	Shipboard description of section		Thin-section description
		Age	Lithology	
165-999A-				
2H-2, 144–150	10.54	Pleistocene	Nannofossil clayey mixed sediment with foraminifers alternating on a dm scale with foraminiferal clayey mixed sediment; structureless overall, slight to moderate bioturbation.	Packstone-wackestone with intraparticle porosity in microfossils.
13H-1, 144-150	113.54	Pliocene	Nannofossil clayey mixed sediment with foraminifers alternating on a dm scale with foraminiferal clayey mixed sediment with nannofossils; homogeneous, massive, slightly to heavily bioturbated.	Bioclast-rich laminated wackestone-packstone. Single microfossils have intraparticle porosity.
35X-5, 144-150	323.44	middle Miocene	Nannofossil clayey mixed sediment with radiolarians; homogeneous, massive, moderately to heavily bioturbated.	Mudstone with single microfossils containing intraparticle porosity.
45X-4, 50-57	417.10	early-middle Miocene	Clayey nannofossil chalk with foraminifers, homogeneous, massive, slightly to heavily bioturbated.	Wackestone-packstone. The frequent microfossils have intraparticle porosity.
61X-1, 78-84	557.28	early Miocene	Clayey calcareous chalk with nannofossils and foraminifers; homogeneous, massive, and moderately bioturbated.	Wackestone. The microfossils are partly cemented, partly containing intraparticle porosity.
165-1001B-				
1R-2, 0-6	26.80	Pleistocene	Nannofossil, clayey mixed sediment with foraminifers; massive, moderately bioturbated, with foraminifers concentrated within burrows.	Packstone with intraparticle porosity in microfossils.
2R-2, 0-6	151.80	middle Miocene	Nannofossil ooze with clay; massive and moderately bioturbated.	Laminated mudstone-wackestone with single shell fragments. No visible intraparticle porosity.
3R-1, 30-36	206.80	early Eocene	Calcareous chalk with clay. The sediment is massive and moderately bioturbated	Wackestone with single microfossils containing intraparticle porosity.
13R-2, 75-81	304.85	late Paleocene	Calcareous chalk with clay; massive, well indurated, moderately bioturbated, and contains burrows flattened by compaction, producing wispy lamination. Coarse-grained foraminifer- and radiolarian-rich intervals present throughout the core. The boundaries of these layers range from transitional to sharp and uneven.	Packstone with microfossils containing intraparticle porosity.
23R-5, 13-19	395.33	Maastrichtian	Calcareous limestone with clay; massive, well indurated, moderately bioturbated, and contains burrows flattened by compaction, producing wispy lamination. There are numerous clay-rich, darker green layers, that are 1–2 cm and have gradational contacts.	Packstone with partly cemented microfossils. Some contain intraparticle porosity.
165-1001A-				
50R-1, 104-110	459.44	Campanian	Calcareous limestone with clay; moderately bioturbated, slightly darker wispy laminated, clay-rich intervals present throughout. Rare foraminifer- and radiolarian-rich sandy horizons with sharp, but nonerosive, boundaries.	Cemented packstone with single intraparticle porosity containing microfossils.

Notes: Shipboard description of section (Sigurdsson, Leckie, Acton, et al., 1997).Thin-section description (Dunham, 1962; Choquette and Pray, 1970).

Table 2. Compaction experiments data, Sites 999 and 1001.

Core, section, interval (cm)	Depth (mbsf)	In situ stress (MPa)	σ max (MPa)	Strain rate ($10^{-6}s^{-1}$)	ε max (%)	Initial φ (%)	φ at ε max (%)	Final φ (%)	φ-curve shift (%)	σ_k' (MPa)	φ rebound (maximal) (%)
165-999A-											
2H-2, 144-150	10.54	0.09	10	3.5	41	71.9	52.4	52.4	0	0.12	0.0
13H -1,144-150	113.54	1.0	21	1	42	65.8	40.9	41.5	4.8	0.4	0.03
35X-5, 144-150	323.44	3	14.5	2.1	34	64.1	45.5	47.6	3.5	3	0.4
45X -4, 50-57	417.1	4	10	2.7	15	60.4	53.4	55.3	-2.1	4	0.7
61X-01, 78-84	557.28	6	16	3.2	8	45.0	40.2	41.9	7.5	6	0.6
165-1001B-											
1R -2, 0-6	26.8	0.3	23	1.3	33	65.1	47.9	42.4	0	1.0	-0.07
2R -2, 0-6	151.8	1.6	17	1.2	33	55.1	33.0	36.4	13.9	0.6	0.3
3R-1, 30-36	206.8	3	40	1.7	29	56.0	38.1	39.6	0.5	3	0.1
13R-2, 75-81	304.85	4	38	1.6	9.4	41.9	35.8	38.4	2.8	9	0.3
23R-5, 13-19	395.33	6	40	1.6	4.2	29.9	26.8	28.2		>40	0.2
165-1001A-											
50R-1, 104-110	459.44	7	42	1.2	11	23.3	13.8	24.9		>40	1.9

Notes: σ = axial stress, ε = strain, φ = porosity, σ_k' = modified axial preconsolidation.

An alternative way of estimating rebound is from comparison of wet bulk density determined in the laboratory and the downhole density log. The wet bulk density should in principle be lower than the logging density by an amount corresponding to the rebound. This strategy proved unsuccessful: the wet bulk density is in every data point larger or equal to the logging density, and no consistent depthwise pattern is seen (Figs. 5, 6). Rather, these data indicate that the downhole density is artificially low, which may occur in a case of excessive hole roughness, whereby the density logging tool obtains a signal from not only the formation but also part of the water-filled hole. Indeed, the caliper logs for Holes 999B and 1001A indicate severe hole roughness (Sigurdsson, Leckie, Acton, et al., 1997).

Preconsolidation and Stylolites

The determination of preconsolidation from the constant rate of strain curves is difficult because the samples were not left to creep at any stress level, and because the applied strain rate of 10^{-6} s^{-1} is high when compared to natural conditions (~10^{-15} s^{-1}). The measured stresses thus become too high relative to the strain (Ruddy et al.,

Table 3. Physical characteristics of samples, Sites 999 and 1001.

Core, section, interval (cm)	Depth (mbsf)	Single point (m^2/g)	BET multipoint (m^2/g)	Per pore volume (m^2/cm^3)	Bulk density (g/cm^3)	I.R. (%)	Grain-size distribution 0.2-0.8 µm (%)	1-5 µm (%)	6-150 µm (%)
165-999A-									
2H-2, 144-150	10.54	23.5	23.9	27	1.55	43.4	48.5	22.3	29.3
13H-1,144-150	113.54	25.1	25.6	37	1.61	37.8	47.1	29.7	23.2
35X-5, 144-150	323.44	54.5	55.1	79	1.56	50.8	38.8	45.9	15.1
45X-4, 50-57	417.10	24.0	24.4	42	1.66	34.6	15.5	31.7	52.7
61X-1, 78-84	557.28	30.9	31.3	93	1.80	28.0	17.6	47.4	34.9
165-1001B-									
1R-2, 0-6	26.80	18.2	18.5	28	1.63	27.6	36.5	20.5	43.2
2R-2, 0-6	151.80	39.5	40.1	85	1.72	47.4	50.6	42.8	6.6
3R-1, 30-36	206.80	6.3	6.5	14	1.80	8.1	12.3	36.8	50.9
13R-2, 75-81	304.85	19.4	19.7	70	1.91	35.2	17.0	34.7	48.5
23R-5, 13-19	395.33	7.4	7.5	47	2.17	12.3	14.2	33.2	52.7
165-1001A-									
50R-1, 104-110	459.44	4.2	4.3	38	2.28	12.5	7.8	29.7	62.5

Notes: BET = specific surface determined by nitrogen adsorption (Brunauer et al., 1938), I.R. = insoluble residue.

Table 4. Specific surface and grain-size data, Leg 130 Site 807.

Core, section, interval (cm)	Depth (mbsf)	BET multipoint (m^2/g)	BET single point (m^2/g)	Grain-size distribution 0.2-0.8 µm (%)	1-5 µm (%)	6-150 µm (%)
130-807A-						
2H-5, 134-140	15	6.2	6.4			
11H-5, 134-140	100	3.7	4.0	24.4	47.0	28.3
22H-6, 134-140	206	3.6	3.9			
34X-5, 134-140	319	3.6	3.7			
44X-4, 137-144	414	3.2	3.4			
76X-4, 43-49	722	3.1	3.2			
86X-1, 131-136	815	2.8	3.1			
130-807C-						
24R-1, 141-147	945	3.2	3.4			

Note: BET = specific surface determined by nitrogen adsorption (Brunauer et al., 1938).

1989). To estimate the preconsolidation for the present samples, Cassagrande's construction, as presented by Jacobsen (1992), was applied: the tangent of the normal consolidated part of the compaction curve crosses the stress axis in the log stress-strain plot in the point σ_k' (Fig. 2). The preconsolidation stress, σ_{pc}', then becomes: $\sigma_{pc}' \approx 2.5\,\sigma_k'$. For simplicity and because of the expected overestimation of stress, the maximal experienced burial stress is estimated by making the modified preconsolidation equal to σ_k'.

Using this estimate, the modified preconsolidation comes close to in situ stress for the samples from Site 999 (Fig. 7). Because no major hiatus is reported in the strata deposited during the period 0–20 Ma (corresponding to the depth interval 0–500 mbsf) at Site 999 (Sigurdsson, Leckie, Acton, et al., 1997), and because the acoustic velocity (Fig. 1) and petrographic description (Table 1) indicate that only the deepest loaded sample is from the zone of initial cementation, the σ_k' probably represents the maximal experienced stress reasonably well and can be used for the interpretation of the burial history of Site 1001.

The modified preconsolidation data for Site 1001 indicate that the three uppermost samples have been subjected to effective burial stresses not significantly larger than the present (Fig. 7; Table 2). The three deepest samples are overconsolidated. Only the topmost of these is shown in Figure 7 because the two deepest samples (from 395 and 459 mbsf) did not yield during the compaction experiments (Fig. 4), and the preconsolidation stress is above the maximally applied 40 MPa. These two samples are both cemented; therefore, chemical processes have probably controlled their present high-yield strength rather than previous deep burial (Pl. 2, Figs. 5, 6). The sample from 304 mbsf is not cemented, as indicated by a high specific surface and from thin sections (Tables 1, 3; Pl. 2, Fig. 4), and it is possible to estimate a modified preconsolidation stress of 9 MPa (Fig. 7; Table 2). By comparison with the present burial stress curve, this suggests a previous burial to ~550 mbsf (250 m deeper). This would also imply that the two deeper samples have been buried to ~650 and 700 mbsf, respectively. By comparison between the acoustic velocity curve for Sites 999 and 1001, this conclusion seems reasonable because a downward shift of 250 m of the curve for Site 1001 brings it to match the curve for Site 999.

The hiatus where the material was removed by erosion should thus be located between the depth of the normally consolidated sample from 206 mbsf and the depth of the overconsolidated sample from 304 mbsf. The paleontological data indicate a minor hiatus at 304 mbsf (Sigurdsson, Leckie, Acton, et al., 1997) (i.e., just above the sample). Hence, it cannot be ruled out that the high preconsolidation may be caused by seafloor induration, although no cementation of microfossils was observed in thin section and no cementation is indicated by the high specific surface (Table 3). The major hiatus of Site 1001 is at 166 mbsf (Sigurdsson, Leckie, Acton, et al., 1997), above the sample collected for loading testing at 206 mbsf, where no significant overconsolidation was found.

The apparent contradiction may be tentatively resolved as follows. The in situ stress curve for Site 1001 is less steep than that defined by Site 999, which may be assumed to be normal because it matches the reference curve for Site 807 down to ~500 mbsf, the depth of the onset of cementation at Site 999 (Fig. 7). If we assume that the shape of the stress curve for Site 1001 reflects an earlier deeper burial, we obtain a match of the curves by shifting the part of the curve below the hiatus at 166 mbsf down by 250 m. This would imply that 250 m + 166 m ≈ 400 m of section is missing above the major hiatus. The modified preconsolidation for a sample from 206 mbsf should by this interpretation be ~4 MPa, not grossly different from the measured 3 MPa, and the sample from 304 mbsf would have

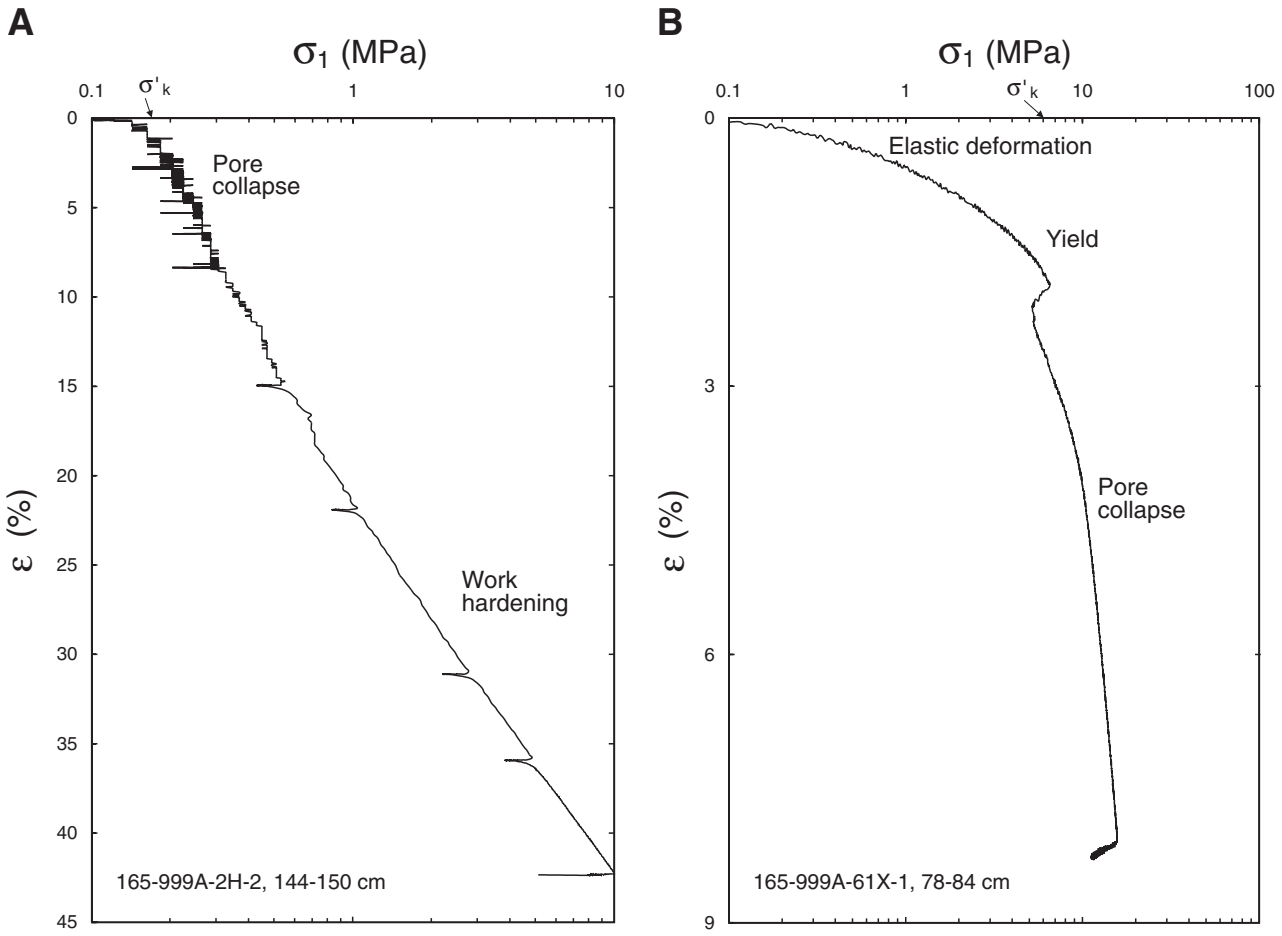

Figure 2. Examples of compaction curves. The resulting strain (ε) is plotted vs. the uniaxial stress (σ_1) on a logarithmic scale. **A.** Sample 165-999A-2H-2, 144–150 cm; 11 mbsf. **B.** Sample 165-999A-61X-1, 78–84 cm; 557 mbsf.

been buried to ~550 mbsf, giving rise to a preconsolidation of 6 MPa, not unreasonably low when compared to the measured 9 MPa. The expected preconsolidation thus becomes lower when it is compared to the burial curve for Site 999 rather than the curve for Site 1001.

No macroscopic stylolites were found in the argillaceous calcareous sediments at Sites 999 and 1001, whereas wispy lamination was commonly observed (Table 5; Pl. 1, Fig. 6; Pl. 3), which follows observations by Bathurst (1987). At Site 999, wispy laminations were noted below 572 mbsf (Sigurdsson, Leckie, Acton, et al., 1997), within the depth range where they are found in the Ontong Java Plateau. At Site 1001, wispy lamination was observed below 305 mbsf (Sigurdsson, Leckie, Acton, et al., 1997). An interpretation that involves a previous burial depth of 550 mbsf for material collected at 304 mbsf thus brings the presence of wispy laminations at Site 1001 in line with respect to burial depth with the observations at Sites 999 and 807, so that all intervals with wispy lamination have been buried to at least 500 mbsf.

The present depths of the first appearance of wispy lamination at Sites 999 and 1001 correspond to depths from which cementation is observed; therefore, a direct link might be expected: material dissolved at the microstylolites precipitates in the matrix as cement. (Micro)stylolites are indeed frequently interpreted to be the source of cement during burial diagenesis (e.g., Choquette and James, 1990; Maliva and Dickson, 1992; Borre and Fabricius, 1998). Dissolution at wispy laminations and stylolitic seams could, from these data alone, be concluded to be associated with the onset of cementation during burial diagenesis, but the observations at the Ontong Java Plateau indicate that this is not the case. At the Ontong Java Plateau, dissolution seams are observed from below a depth of 490 mbsf and stylolites below a depth of 830 mbsf (Lind, 1993b), whereas cementation is observed below 1100 mbsf (Borre and Fabricius, 1998). These observations indicate that the formation of wispy lamination (and probably also macroscopic stylolites) is governed by burial depth, whereas the onset of cementation is also governed by other factors, such as temperature and chemical composition of the pore water (Øxnevad and Meshri, 1997).

Texture, Microfossil Content, and Critical Porosity

For the upper 572 mbsf of Site 999, the sedimentation rate is nearly constant (Sigurdsson, Leckie, Acton, et al., 1997) and the modified preconsolidation stress curve follows the burial stress (Fig. 7). It could, therefore, at first glance seem surprising that the compaction curves in the stress-porosity plot (Fig. 3) do not form a common trend. To understand the cause for this scatter, all compaction curves for deeper samples were shifted along the porosity axis to match the curve for the shallowest sample, and the porosity shift measured (Fig. 8). A similar procedure was followed for the four upper samples of Site 1001, omitting the two deeper tests that did not reach the yield point (Fig. 9). The samples that are porosity shifted the least (Figs. 8, 9) contain the largest content of porous microfossils (Table 1; Pl. 1, Fig. 4; Pl. 2, Figs. 3, 4). The shift is nonproblematic for three of the tests on samples from Site 1001, and for four of the tests representing Site 999. For each of these tests, the trend lines follow the same curve of normal consolidation subsequent to yielding. The shift in compaction curves along the porosity axis indicates a common ideal initial porosity of 72%, as represented by the initial porosity of the sample from 11 mbsf at Site 999, and thus represents a slightly higher seafloor porosity. The

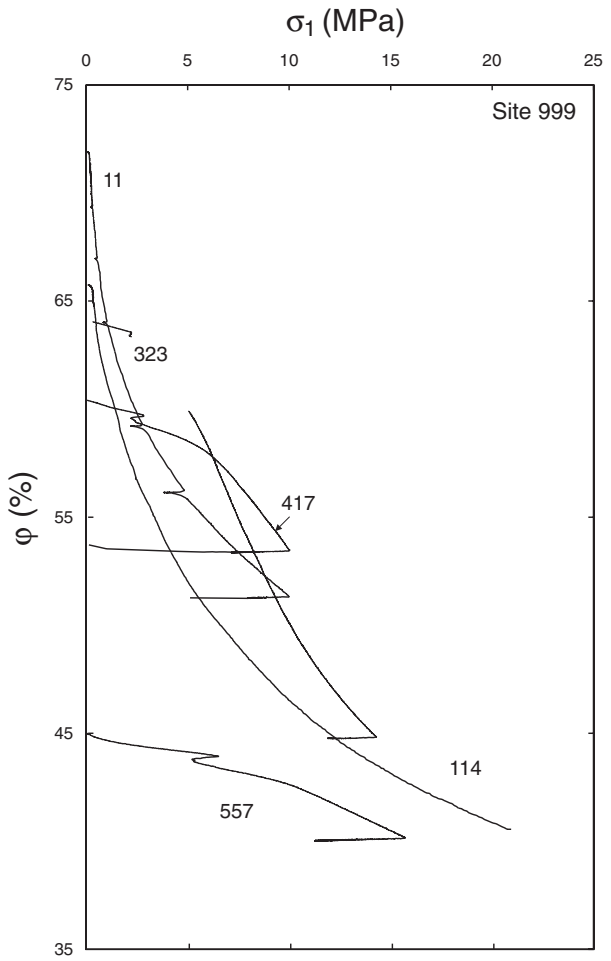

Figure 3. Compaction curves showing uniaxial stress (σ_1) vs. porosity (φ) for all samples from Site 999. Sample depths are labeled in meters below seafloor.

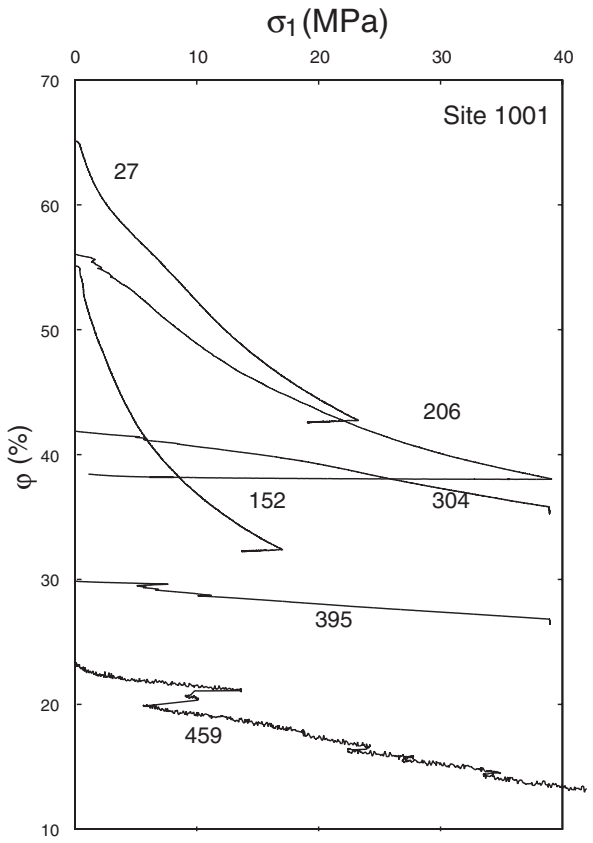

Figure 4. Compaction curves showing uniaxial stress (σ_1) vs. porosity (φ) for all samples from Site 1001. Sample depths are labeled in meters below seafloor.

sample from 114 mbsf at Site 999 contains only a little intraparticle porosity (Table 1; Pl. 1, Fig. 2); thus, the porosity shift of 5% for this sample suggests that the ideal initial seafloor porosity is composed of 5% intraparticle porosity and 67% matrix porosity. The compaction curves for the sample from 323 mbsf at Site 999 and the sample from 152 mbsf at Site 1001 (Pl. 1, Fig. 3; Pl. 2, Fig. 2) break the overall pattern. The normal-consolidated part of the curve for these samples shows a larger porosity decrease for a given increase in stress than the other samples.

I chose the compaction curves for the fine-grained carbonate matrix of Site 807 (Lind, 1993a) as a reference for the interpretation of the compaction curves obtained from Sites 999 and 1001 because of the relative uniformity of the calcareous ooze and chalk of the Ontong Java Plateau. The relatively pure carbonate lithology at Site 807 is reflected in a relatively low and constant specific surface of the material (Table 4; Fig. 10). The common trend line for Site 1001 falls relatively close to the trend in matrix porosity of calcareous ooze, as defined for the tests for Site 807, whereas the trend line for Site 999 is shifted to higher porosities (Figs. 8, 9). This difference is an artifact of the shifting procedure, and the trend lines may be matched by additional shifting. This indicates that the microfossils play only an insignificant role in the compaction pattern and that, despite the generally high clay content of the Caribbean samples, the compaction curves follow the pattern from Site 807 in the Ontong Java Plateau.

Regarding the composition of the samples, the two deepest limestone samples from Site 1001 and the chalk from 206 mbsf at Site 1001 have specific surfaces comparable to the samples from Site 807, and the three samples are characterized by a relatively high carbonate content as reflected in insoluble residues between 8% and 12% (Table 3). The remaining samples have high insoluble residues and corresponding high specific surfaces. The dominance of clay in the insoluble residue of the samples is thus demonstrated by the positive correlation between insoluble residue and specific surface (Fig. 11). The samples that follow the compaction trend of Site 807 have a three-modal pattern in grain-size distribution; thus, all data are represented by three classes of sizes (Fig. 12). The similarity in compaction trends thus indicates that the compaction is controlled by the fine-grained calcite, whereas the larger microfossils are passive, and the fine-grained clay fraction is dispersed in the pore fluid. The latter effect may be possible because the water-bearing clay is dispersed in the pores between the carbonate particles, rather than concentrated in layers.

Even if dispersed, the clay is in some cases the dominating constituent: the two samples with distinct compaction patterns (from 323 mbsf at Site 999 and from 152 mbsf at Site 1001) are characterized by a small proportion of larger grains, by their mudstone texture (Table 1; Pl. 1, Fig. 3: Pl. 2, Fig. 2), and by their large insoluble residue and specific surface (Table 3). The large porosity reduction for these samples for a given stress increase is thus probably a consequence of the near bimodal packing of fine carbonate particles and the slightly more dominating clay (Fig. 12, Sections 165-999A-35X-5, and 165-1001B-2R-2), so that the compaction of these samples is controlled by the fine-grained clay fraction. The logic behind this explanation is that clay should compact easier than carbonate ooze, resulting in a larger porosity reduction for a given increase in uniaxial stress.

The above interpretation is the same as the critical porosity model of Nur et al. (1995). In newly deposited sediment near the seafloor, the grain-size fraction that supports the grain structure contains its

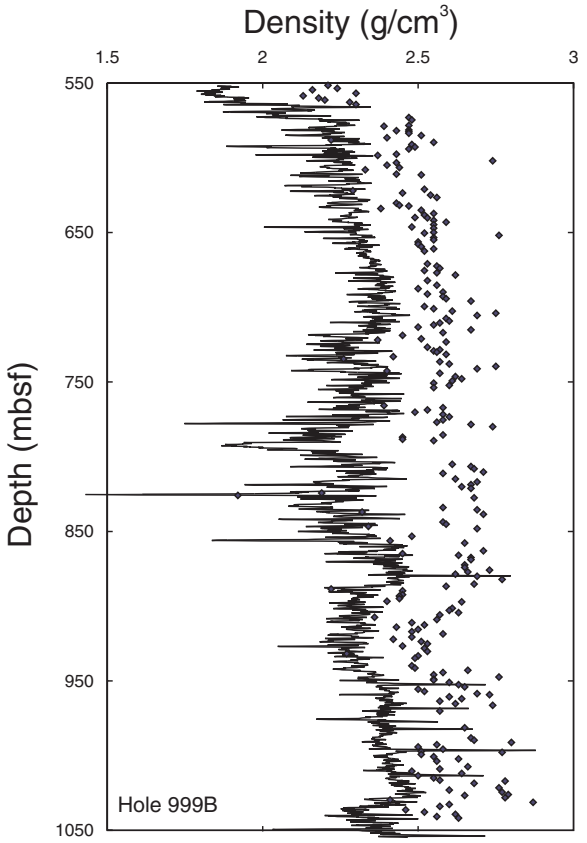

Figure 5. Density downhole logging data (solid line) compared to laboratory wet bulk densities of discrete samples (diamonds) for Hole 999B (data from Sigurdsson, Leckie, Acton, et al., 1997).

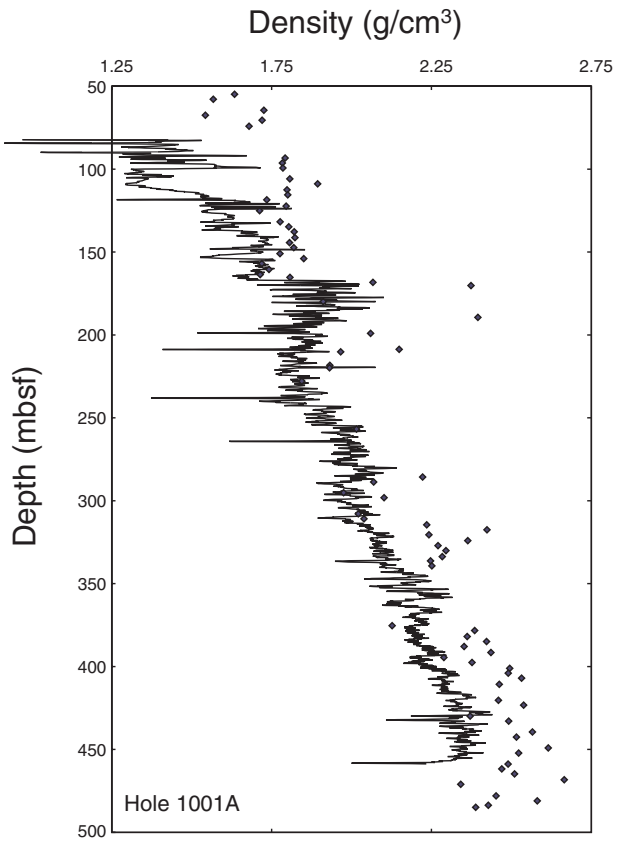

Figure 6. Density downhole logging data (solid line) compared to laboratory wet bulk densities of discrete samples (diamonds) for Hole 1001A (data from Sigurdsson, Leckie, Acton, et al., 1997).

maximal (critical) porosity. Higher porosities would imply that the entire material is in suspension. Finer grained material in suspension in the pores does not contribute to the mechanical stability of the frame. The studied material from the Caribbean Sites 999 and 1001 fit this pattern, probably because of the dispersed nature of the fine-grained particles. This may also explain the unexpected results of Lind (1997): relatively low porosities corresponding to a given traveltime and an overall linear relationship between acoustic traveltime and porosity was found for Leg 165 samples (Sigurdsson, Leckie, Acton, et al., 1997) in the entire porosity interval from <10% to >70% irrespective of carbonate content. This indicates a practically constant governing texture reflected in a critical porosity of 73% for all samples (Fig. 13). Similarly, for the purer chalk facies sediments of the Ontong Java Plateau, a practically constant critical porosity of 68% was indicated by the near linear acoustic traveltime porosity trend (Lind, 1997).

CONCLUSIONS

1. No significant rebound effects have been demonstrated in the porous, upper soft sediment section of Sites 999 and 1001, whereas a rebound in porosity of ~2% is estimated for the cemented, deeper sections below 572 mbsf at Site 999 and below 352 mbsf at Site 1001.
2. By a modified strategy for determination of preconsolidation from consolidation tests, preconsolidations matching the present burial stress were obtained for the upper 550 m of soft sediments at Site 999, in accordance with the conservative burial history indicated for this site by paleontological data (Sigurdsson, Leckie, Acton, et al., 1997).
3. By applying the same strategy to compaction curves from Site 1001, and from interpretation of the present in situ burial stress -depth curve, 400 m of section is estimated to be missing at the hiatus at 166 mbsf at Site 1001. This interpretation of previous burial at Site 1001 brings the occurrence of wispy laminations with respect to burial depth in agreement with their occurrence at Sites 999 and 807. Based on this interpretation, the burial depth for the first appearance of wispy lamination at the three sites is ~500 mbsf.
4. At Sites 999 and 1001, wispy laminations are observed over the same depth ranges as cementation is observed, and a direct link between dissolution and precipitation might be suggested. Data from Site 807 suggest no direct link because dissolution seams and stylolites are observed ~500 and ~300 m, respectively, above the depth where cementation is found. These observations indicate that the formation of wispy lamination and stylolites is governed by burial depth, whereas the onset of cementation is governed by other factors (e.g., temperature and chemical composition of the pore water).
5. The slopes of the compaction curves are similar for the relatively carbonate-rich samples studied and are comparable to calcareous sediments from Site 807. Each compaction curve has a distinct shift along the porosity axis. This is interpreted to be because of microfossils playing only an insignificant passive role during compaction. Despite the generally high clay content of these Caribbean samples (8%–43% insoluble residue), the compaction curves are controlled by the fine-grained calcite, so that the fine-grained clay fraction appears to be moving dispersed in the pore fluid between the calcite grains.
6. Two relatively clay rich (47% and 50% insoluble residue) and microfossil poor samples underwent relatively large porosity

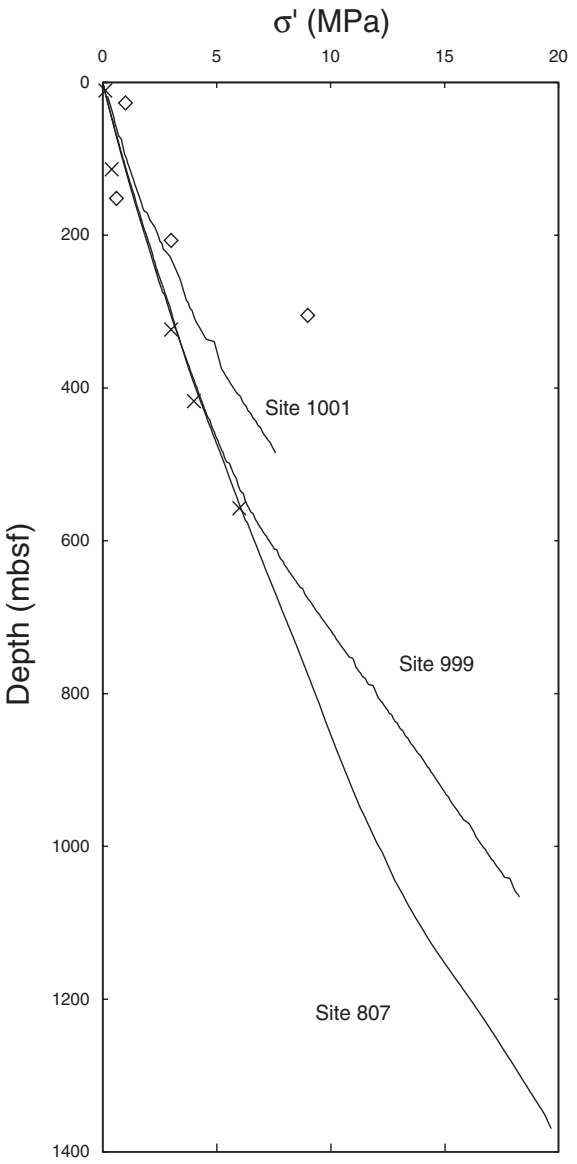

Figure 7. Present vertical effective stress (σ') vs. burial, calculated from laboratory wet bulk densities of discrete samples for Sites 999, 1001, and 807 (data from Kroenke, Berger, Janecek, et al., 1991, and Sigurdsson, Leckie, Acton, et al., 1997). Modified preconsolidation: $\sigma_k' \approx \sigma_{pc}'$/ 2.5, as determined from loading experiments, are marked by crosses (Site 999) and diamonds (Site 1001).

Table 5. Occurrence of stylolites and microstylolites, Sites 806, 807, 999, and 1001.

	Site 806	Site 807	Site 999	Site 1001
First microstylolites	630	490	572	305
First stylolites		830		

Notes: Occurrence shown in meters below seafloor. Sites 806, 807 (Kroenke, Berger, Janecek, et al., 1991; Lind, 1993b), Sites 999 and 1001 (Sigurdsson, Leckie, Acton, et al., 1997).

loss during loading. This is probably a consequence of the bimodal distribution of fine carbonate particles and clay. The compaction of these samples appears to be controlled mainly by the fine-grained clay fraction.

ACKNOWLEDGMENTS

Samples and data for this paper were collected by the Shipboard Scientific Party during ODP Leg 165. The support from the shipboard technical staff is acknowledged, as well as that from K. Carlsen, H. Diàz, B. Frydenlund, S.H. Nguyen, V. Knudsen, and T. Valerius, all from the Technical University of Denmark (DTU); M.K. Borre, DTU; H. Machel, University of Alberta; and E. Mountjoy, Geological Survey of Canada, are thanked for critically reading the text.

REFERENCES

Audet, D.M., 1995. Modelling of porosity evolution and mechanical compaction of calcareous sediments. *Sedimentology,* 42:355–373.

Bathurst, R.G.C., 1987. Diagenetically enhanced bedding in argillaceous platform limestones: stratified cementation and selective compaction. *Sedimentology,* 34:749–778.

Borre, M., and Fabricius (Lind), I.L., 1998. Chemical and mechanical processes during burial diagenesis of chalk: an interpretation based on specific surface data of deep-sea sediments. *Sedimentology,* 45:755–770.

Brunauer, S., Emmett, P.H., and Teller, E., 1938. Adsorption of gasses in multimolecular layers. *J. Am. Chem. Soc.,* 60:309–319.

Choquette, P.W., and James, N.P., 1990. Carbonate diagenesis on the modern and ancient sea floor, meteoric diagenesis and diagenesis in the zone of mixed waters. *In* Grane, R.B., and Hadley, M.G. (Eds.), *The Development of Porosity in Carbonate Reservoirs: Short Course Notes.* Can. Soc. Pet. Geol., 1.1–1.63.

Choquette, P.W., and Pray, L.C., 1970. Geologic nomenclature and classification of porosity in sedimentary carbonates. *AAPG Bull.,* 54:207–250.

Dunham, R.J., 1962. Classification of carbonate rocks according to depositional texture. *In* Ham, W.E. (Ed.), *Classification of Carbonate Rocks.* AAPG Mem., 108–121.

Garrison, R.E., and Kennedy, W.J., 1977. Origin of solution seams flaser structure in Upper Cretaceous chalks of southern England. *Sediment. Geol.,* 19:107–137.

Hamilton, E.L., 1976. Variations of density and porosity with depth in deep-sea sediments. *J. Sediment. Petrol.,* 46:280–300.

Hamilton, E.L., Bachman, R.T., Berger, W.H., Johnson, T.C., and Mayer, L.A., 1982. Acoustic and related properties of calcareous deep-sea sediments. *J. Sediment. Petrol.,* 52:733–753.

Jacobsen, H.M., 1972. New Oedometer and new triaxial apparatus for firm soils. *Dan. Geotech. Inst. Bull.,* 27:7–20.

————, 1992. Bestemmelse af forbelastningstryk i laboratoriet. *Proc. NGM 92, Aalborg.* dgf-Bull., 9:455–460.

Kim, D.-C., Manghnani, M.H., and Schlanger, S.O., 1985. The role of diagenesis in the development of physical properties of deep-sea carbonate sediments. *Mar. Geol.,* 69:69–91.

Kroenke, L.W., Berger, W.H., Janecek, T.R., et al., 1991. *Proc. ODP, Init. Repts.,* 130: College Station, TX (Ocean Drilling Program).

Lind, I., 1997. A modified Wyllie equation for the relationship between porosity and sonic velocity of mixed sediments and carbonates from the Caribbean Sea. *In* Middleton, M.F. (Ed.), *Nordic Petroleum Technology.* Res. Pet. Technol. Ser., 3:123–137.

Lind, I.L., 1993a. Loading experiments on carbonate ooze and chalk from Leg 130, Ontong Java Plateau. *In* Berger, W.H., Kroenke, L.W., Mayer, L.A., et al., *Proc. ODP, Sci. Results,* 130: College Station, TX (Ocean Drilling Program), 673–686.

————, 1993b. Stylolites in chalk from Leg 130, Ontong Java Plateau. *In* Berger, W.H., Kroenke, L.W., Mayer, L.A., et al., *Proc. ODP, Sci. Results,* 130: College Station, TX (Ocean Drilling Program), 445–451.

Maliva, R.G., and Dickson, J.A.D., 1992. Microfacies and diagenetic controls of porosity in Cretaceous/Tertiary chalks, Eldfisk Field, Norwegian North Sea. *AAPG Bull.,* 76:1825–1838.

Masters, J.C., and Maghnani, M.H., 1993. Consolidation test results and porosity rebound of Ontong Java Plateau sediments. *In* Berger, W.H., Kroenke, L.W., Mayer, L.A., et al., *Proc. ODP, Sci. Results,* 130: College Station, TX (Ocean Drilling Program), 687–693.

Mayer, L.A., 1979. Deep sea carbonates: acoustic, physical, and stratigraphic properties. *J. Sediment. Petrol.,* 49:819–836.

Moran, K., 1997. Elastic property corrections applied to Leg 154 sediment, Ceara Rise. *In* Shackleton, N.J., Curry, W.B., Richter, C., and Bralower, T.J. (Eds.), *Proc. ODP, Sci. Results,* 154: College Station, TX (Ocean Drilling Program), 151–155.

Nur, A., Mavko, G., Dvorkin, J., and Gal, D., 1995. Critical porosity: the key to relating physical properties to porosity in rocks. *65th Ann. Intl. Mtg. Soc. Explor. Geophys.,* extended abstracts: 878–881.

Øxnevad, I.E.I, and Meshri, I.D., 1997. Porosity evolution in chalks: crestal Valhall and flank areas. *59th EAEG Conf. Tech. Exhib.,* extended abstracts book, 552.

Ruddy, I., Andersen, M.A., Patillo, P.D., Bishlawi, M., and Foged, N., 1989. Rock compressibility, compaction, and subsidence in a high-porosity chalk reservoir: a case study of Valhall field. *J. Pet. Technol.,* July 1989:741–746.

Schlanger, S.O., and Douglas, R.G., 1974. The pelagic ooze-chalk-limestone transition and its implication for marine stratigraphy. *In* Hsü, K.J., and Jenkyns, H.C. (Eds.), *Pelagic Sediments: On Land and Under the Sea.* Spec. Publ. Int. Assoc. Sedimentol., 1:117–148.

Scholle, P.A., 1977. Chalk diagenesis and its relation to petroleum exploration: oil from chalks, a modern miracle? *AAPG Bull.,* 61:982–1009.

Sigurdsson, H., Leckie, R.M., Acton, G.D., et al., 1997. *Proc. ODP, Init. Repts.,* 165: College Station, TX (Ocean Drilling Program).

Urmos, J., Wilkens, R.H., Bassinot, F., Lyle, M., Marsters, J.C., Mayer, L.A., and Mosher, D.C., 1993. Laboratory and well-log velocity and density measurements from the Ontong Java Plateau: new in-situ corrections to laboratory data for pelagic carbonates. *In* Berger, W.H., Kroenke, L.W., Mayer, L.A., et al., *Proc. ODP, Sci. Results,* 130: College Station, TX (Ocean Drilling Program), 607–622.

Date of initial receipt: 15 July 1998
Date of acceptance: 29 April 1999
Ms 165SR-006

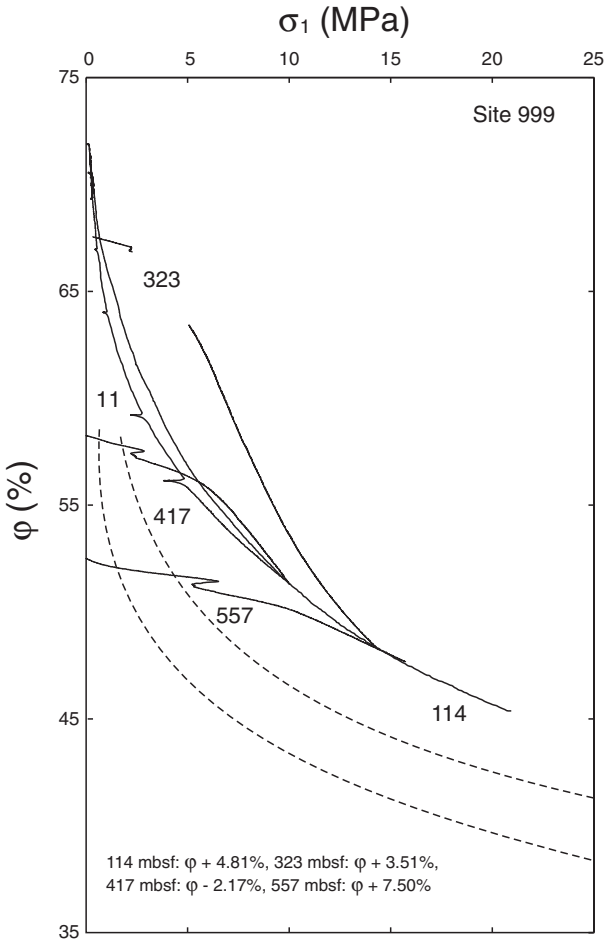

Figure 8. Compaction curves showing uniaxial stress (σ_1) vs. porosity (φ) for samples from Site 999. Sample depths are labeled in meters below seafloor. The curves for the deeper samples (114, 323, 417, and 557 mbsf) have been shifted along the porosity axis to meet the curve defined by the shallowest sample (11 mbsf). The dashed reference curves are matrix compaction curves for Site 807 (Lind, 1993a).

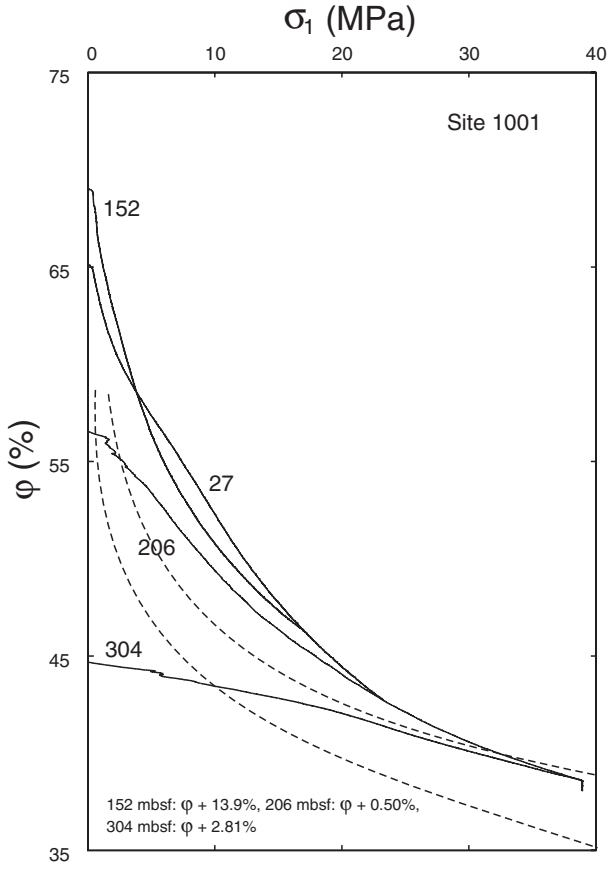

Figure 9. Compaction curves showing uniaxial stress (σ_1) vs. porosity (φ) for samples from Site 1001. Sample depths are labeled in meters below seafloor. The curves for the deeper samples (152, 206, and 304 mbsf) have been shifted along the porosity axis to meet the curve defined by the shallowest sample (27 mbsf). The dashed reference curves are matrix compaction curves for Site 807 (Lind, 1993a).

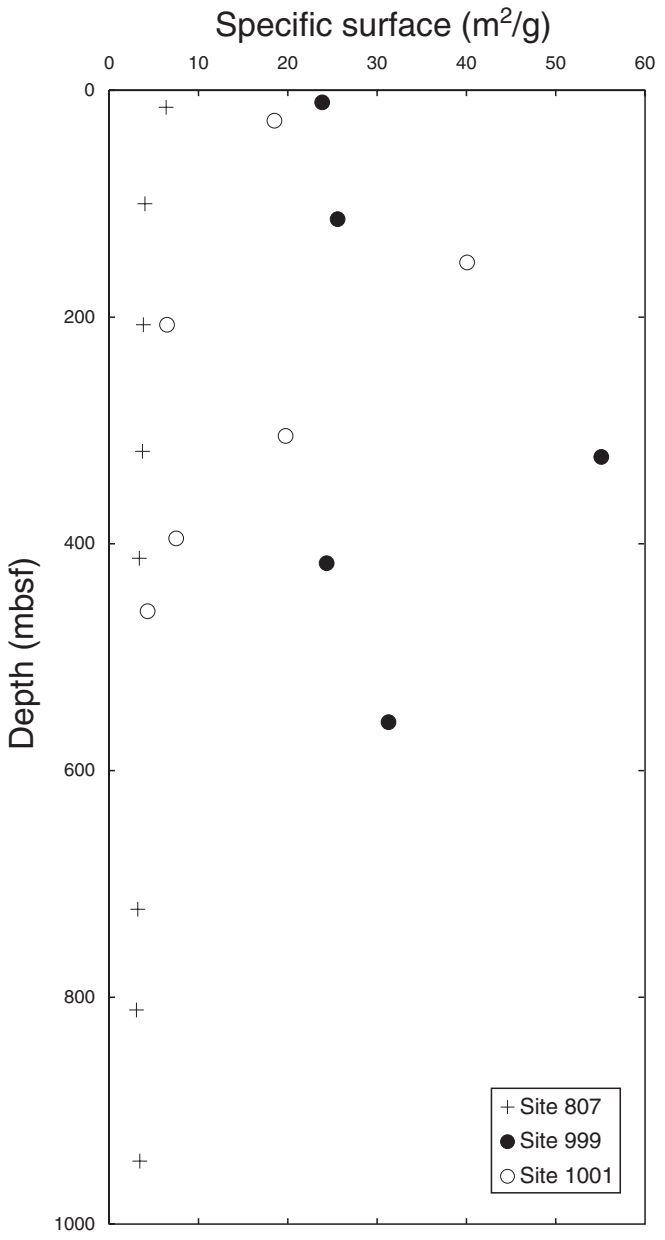

Figure 10. Specific surface as determined by nitrogen adsorption (BET multipoint) vs. depth for samples from Sites 999 and 1001 after compaction experiments. Data for compacted samples from Site 807 are shown as a reference.

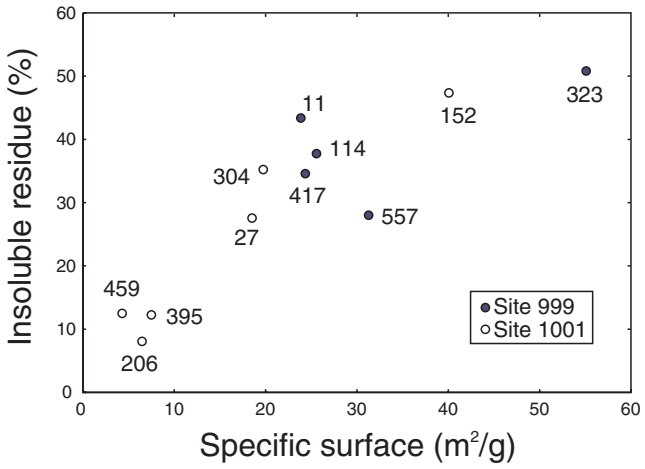

Figure 11. Insoluble residue vs. specific surface as determined by nitrogen adsorption (BET multipoint) for samples from Sites 999 and 1001 after compaction experiments. Sample depths are labeled in meters below seafloor.

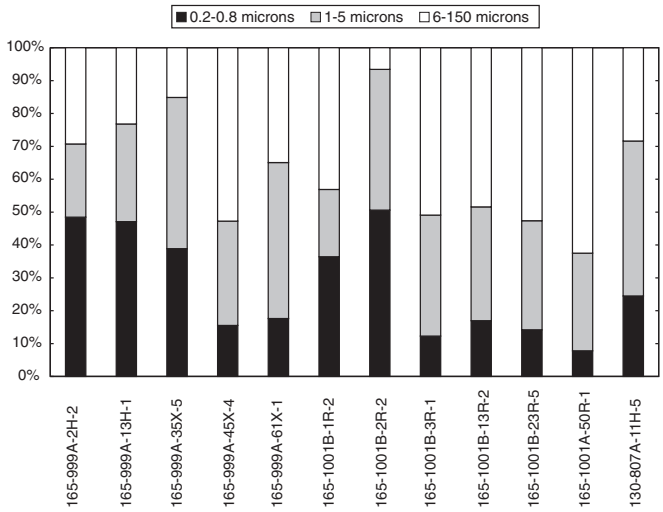

Figure 12. Grain-size distribution of samples from Sites 999 and 1001 after compaction experiments. A single compacted sample from Site 807 is included for reference.

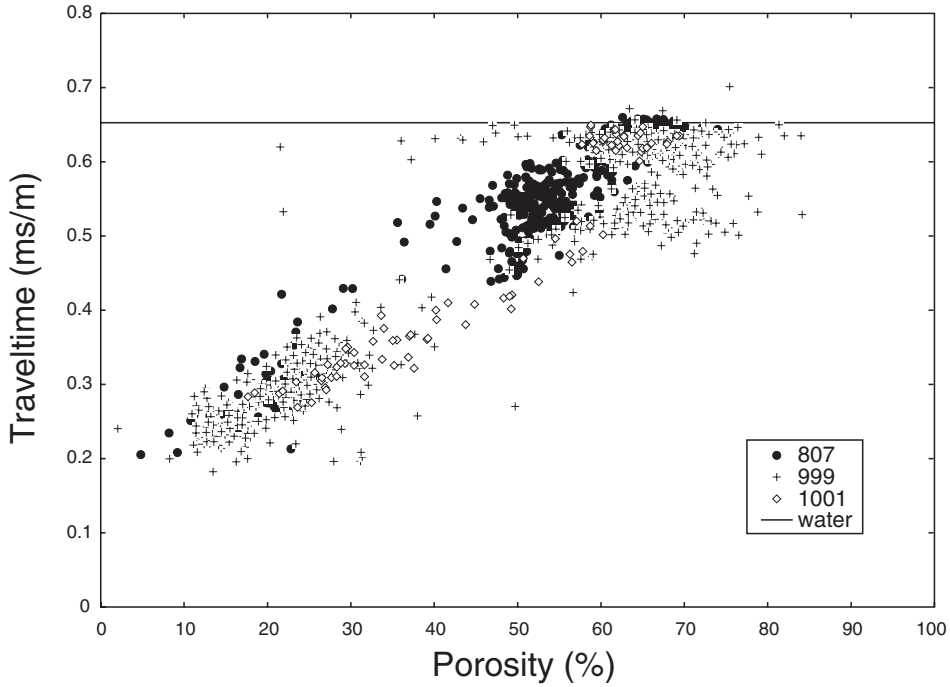

Figure 13. Sonic transit time (the inverse of sonic velocity) vs. porosity for samples from Sites 999, 1001, and 807. The sonic transit time of salt water is shown as a reference. (Data from Kroenke, Berger, Janecek, et al., 1991, and Sigurdsson, Leckie, Acton, et al., 1997).

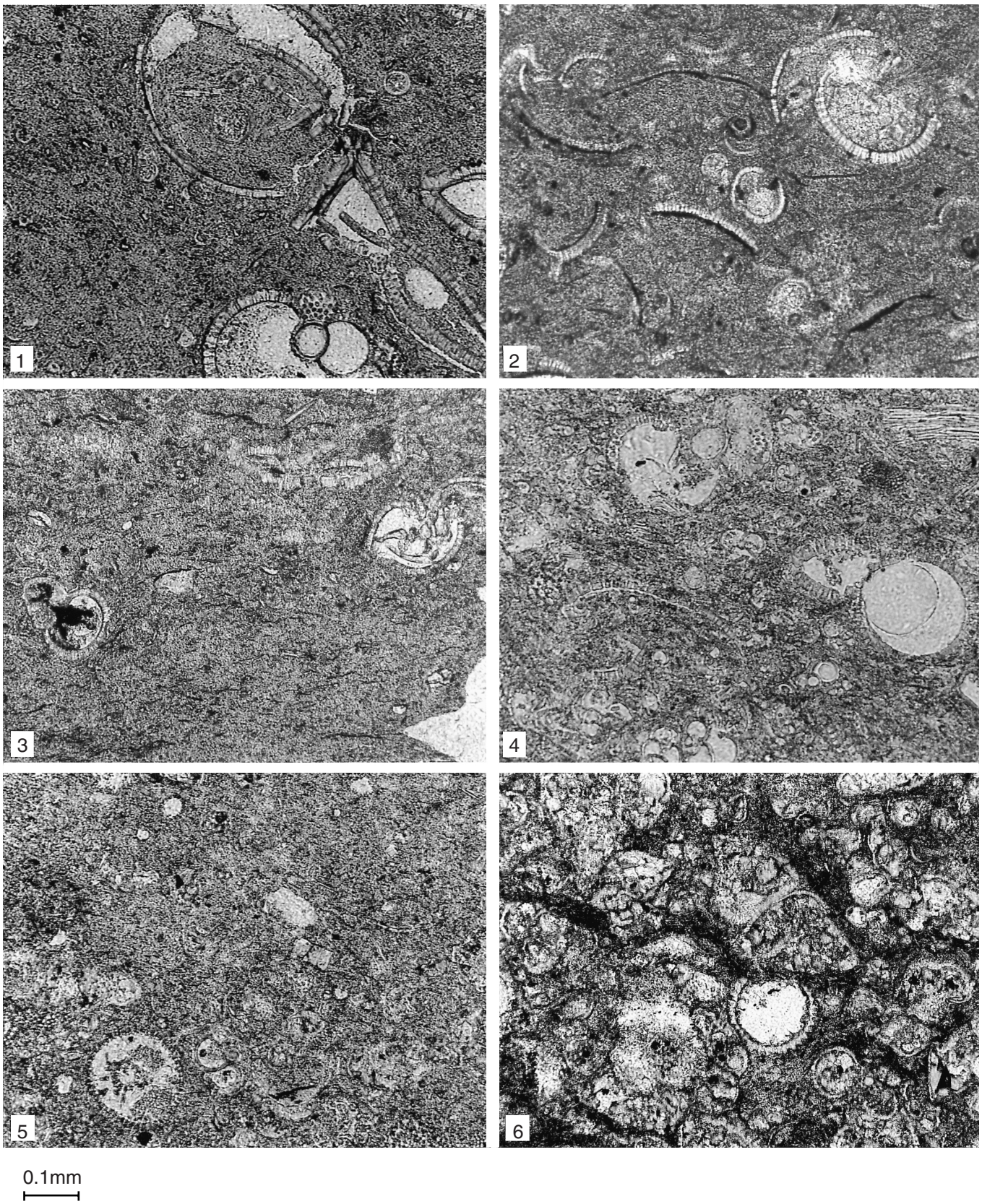

Plate 1. Thin-section photomicrographs of samples from Site 999 subsequent to compaction experiments and a micrograph of wispy lamination. **1.** Sample 165-999A-2H-2, 144–150 cm. **2.** Sample 165-999A-13H-1, 144–150 cm. **3.** Sample 165-999A-35X-5, 144–150 cm. **4.** Sample 165-999A-45X-4, 50–57 cm. **5.** Sample 165-999A-61X-1, 78–84 cm. **6.** Wispy lamination; Sample 165-999B-57R-1, 34–36 cm (see Plate 3).

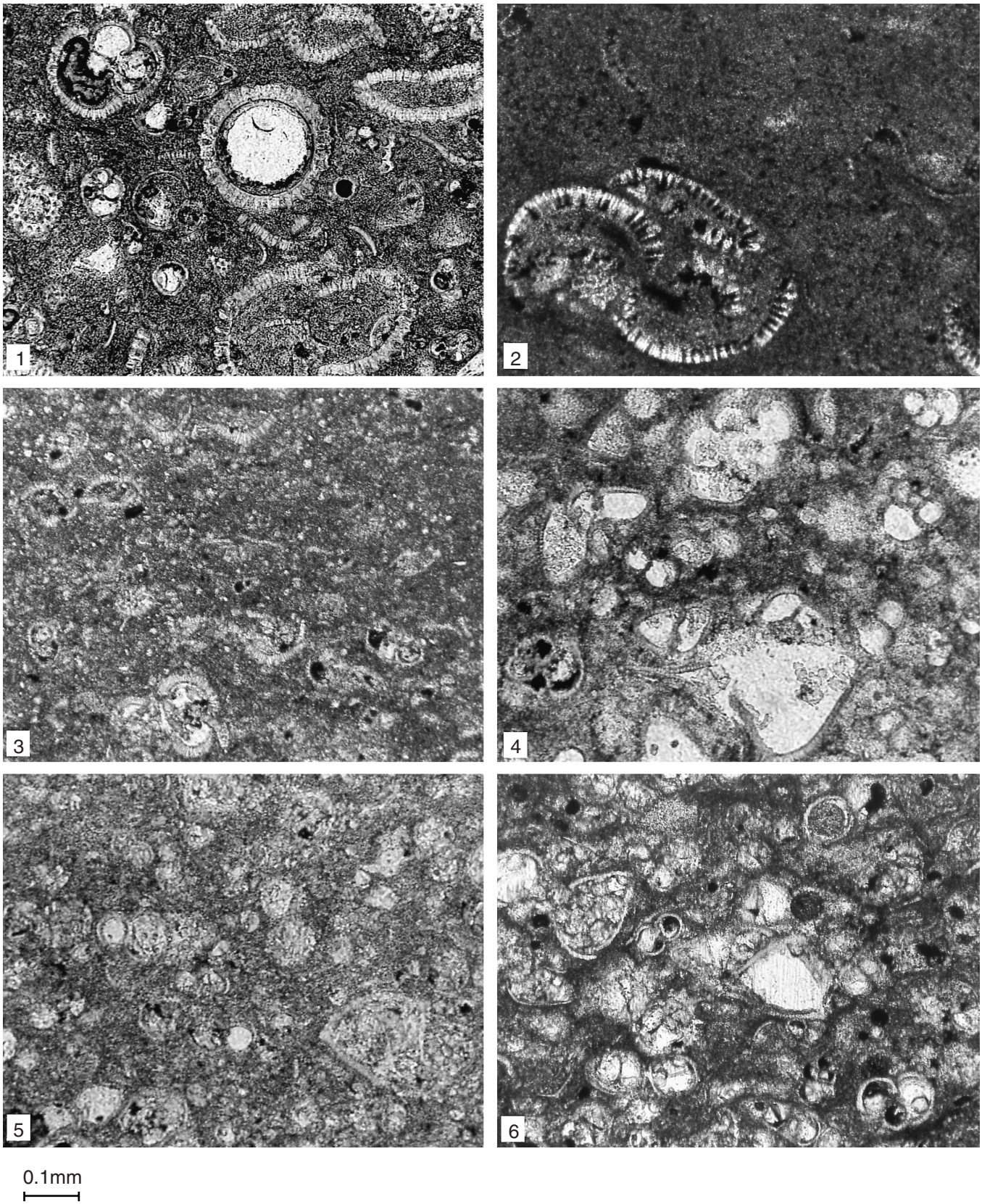

Plate 2. Thin-section photomicrographs of samples from Site 1001 subsequent to compaction experiments. **1.** Sample 165-1001B-1R-2, 0–6 cm. **2.** Sample 165-1001B-2R-2, 0–6 cm. **3.** Sample 165-1001B-3R-1, 30–36 cm. **4.** Sample 165-1001B-13R-2, 75–81 cm. **5.** Sample 165-1001B-23R-5, 13–19 cm. **6.** Sample 165-1001A-50R-1, 104–110 cm.

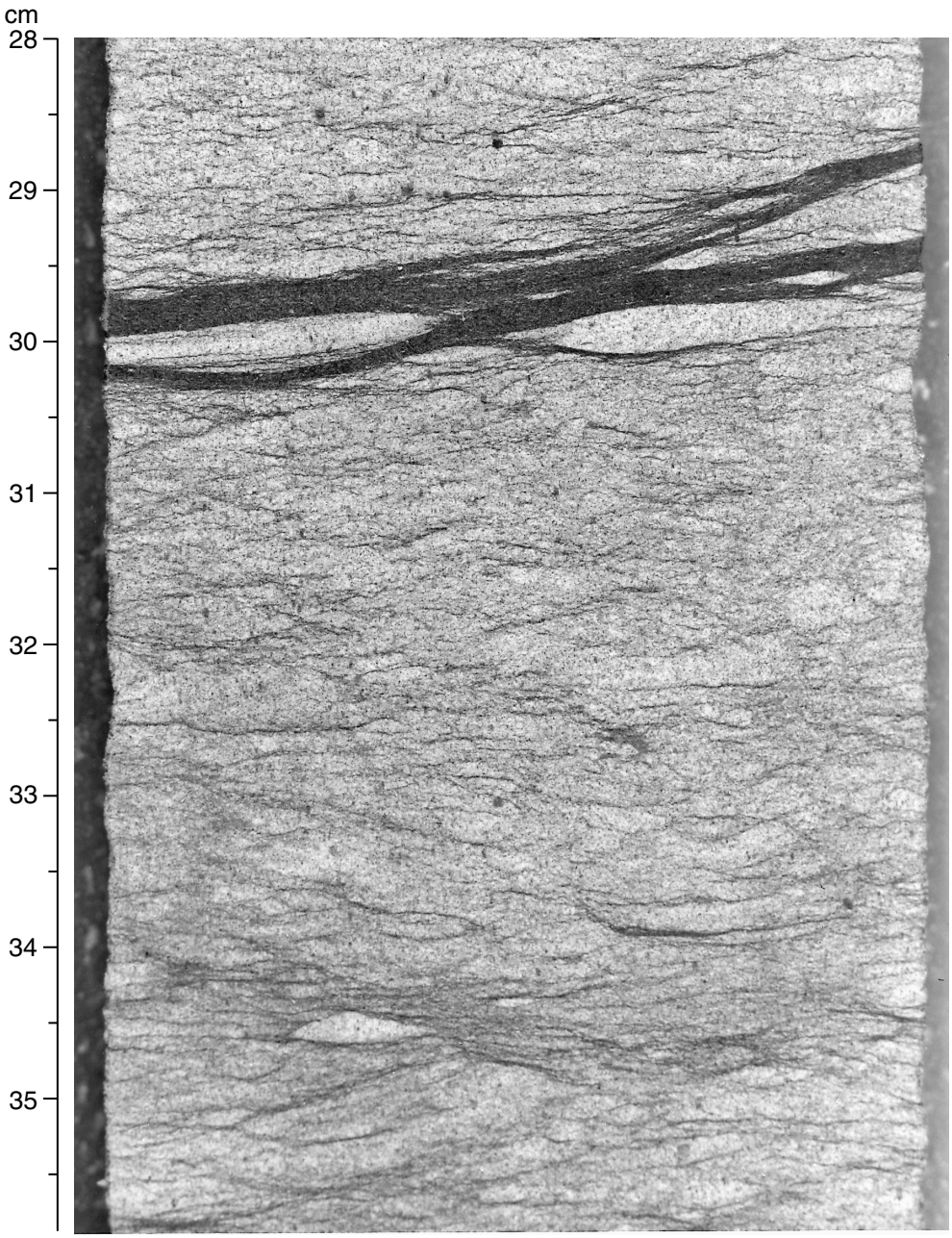

Plate 3. Wispy laminations in Paleocene clayey calcareous mixed sedimentary rock (Sample 165-999B-57R-1, 28–36 cm; 1026 mbsf).